

Revisiting Temporal Modeling for Video Super-resolution

Takashi Isobe¹
tjbj18@mails.tsinghua.edu.cn

Fang Zhu²
zhuf14@gmail.com

Xu Jia³
xujia@huawei.com

Shengjin Wang¹
wsgsj@tsinghua.edu.cn

¹ Department of Electronic Engineering,
Tsinghua University

² Department of Computer Engineering,
New York University,
11201, USA

³ Noah's Ark Lab,
Huawei Technologies

Abstract

Video super-resolution plays an important role in surveillance video analysis and ultra-high-definition video display, which has drawn much attention in both the research and industrial communities. Although many deep learning-based VSR methods have been proposed, it is hard to directly compare these methods since the different loss functions and training datasets have a significant impact on the super-resolution results. In this work, we carefully study and compare three temporal modeling methods (2D CNN with early fusion, 3D CNN with slow fusion and Recurrent Neural Network) for video super-resolution. We also propose a novel Recurrent Residual Network (RRN) for efficient video super-resolution, where residual learning is utilized to stabilize the training of RNN and meanwhile to boost the super-resolution performance. Extensive experiments show that the proposed RRN is highly computational efficiency and produces temporal consistent VSR results with finer details than other temporal modeling methods. Besides, the proposed method achieves state-of-the-art results on several widely used benchmarks. Code is available at <https://github.com/junpan19/RRN>.

1 introduction

Super-resolution is a traditional yet still dynamic topic in low-level vision field, which aims at producing a high-resolution image from the corresponding low-resolution counterparts. It has drawn much attention in recent years due to the increasing demand in mobile phones and ultra-high-definition displays. Single-image super-resolution (SISR) has achieved significant improvements over the last few years, which benefits greatly from progress in deep learning. Recently, more attentions have been shifted to the video super-resolution (VSR) since a video sequence should contain more abundant information. In contrast with SISR, which relies on natural image priors and self-similarity within images for recovering the missing details, VSR is able to utilize additional temporal information from the neighboring frames for further improving the quality of SR.

Previous VSR works divide into two categories: 1) explicit motion compensation based

methods [10, 13, 20, 23, 26] and 2) implicit motion compensation based methods [9, 8, 12, 16, 25, 27]. As for explicit motion compensation based methods, Kappeler *et al.* proposes to warp all neighboring frames to the reference frame based on the offline estimated optical flow; VESCPN [10] is the first end-to-end video SR method by jointly training optical flow estimation and spatial-temporal networks. However, these works are not ideal for VSR since inaccurate motion estimation and alignment would result in errors and deteriorated super-resolution performance. Besides, the computation of optical flow often introduces heavy computational load, which restricts deploying these methods in real systems.

Another branch of VSR explores advanced temporal modeling frameworks to utilize motion information in an implicit manner. Typically, these temporal modeling frameworks have been widely used: 2D with early fusion CNN [8, 24, 25, 27], 3D CNN with slow fusion [11, 12, 16] and Recurrent Neural Network (RNN) [9, 8, 10, 20].

Although extensive experiments have been reported on the aforementioned methods, it is hard to directly compare the effectiveness of these temporal modeling approaches because they adopt different training sets and loss functions to develop their model, which significantly influences the quality of the estimated high-resolution frames. For example, [12] trained their model on the private dataset and supervised an elaborately designed Huber Loss. [8] developed their model on Vimeo-90k [26] dataset and supervised by \mathcal{L}_1 Loss. Moreover, different network depth also limits the direct comparison among these temporal modeling methods, *e.g.* [12] adopted 52 layers in their large model and [25] exploited more deep network.

In this paper, we comprehensively investigate the effectiveness of different temporal modeling approaches on the VSR task by using the fixed loss function (\mathcal{L}_1 Loss) and training data. Specifically, we explore three commonly used temporal modeling methods: 1) 2D CNN with early fusion, 2) 3D CNN with slow fusion and 3) RNN. Inspired by [18], we design the 2D CNN with several modified 2D residual blocks. As for 3D CNN, we further modify these 2D residual blocks to 3D residual blocks. We also incorporate such residual connection into the hidden state of the recurrent network and propose Recurrent Residual Network (RRN) for video super-resolution. In the proposed hidden state, the identity branch not only carries rich image details from the previous layers to the next layers but also helps to avoid gradient vanishing in RNN training. For fair comparison of these temporal modeling methods, we evaluate these models on widely used benchmarks with the same network depth. The experimental results show that Recurrent-based methods are highly efficient and effective in dealing with the VSR problem. Besides, the proposed RRN achieves state-of-the-art performance on three benchmarks.

To sum up, we make the following contributions:

- We carefully study three commonly used temporal modeling methods (2D CNN with early fusion, 3D CNN with slow fusion, and RNN) for the VSR problem.
- We propose a novel hidden state for the recurrent network, which achieves the best performance among all temporal modeling methods. To more surprise, the proposed method outperforms the previous state-of-the-art methods on all three public benchmarks.

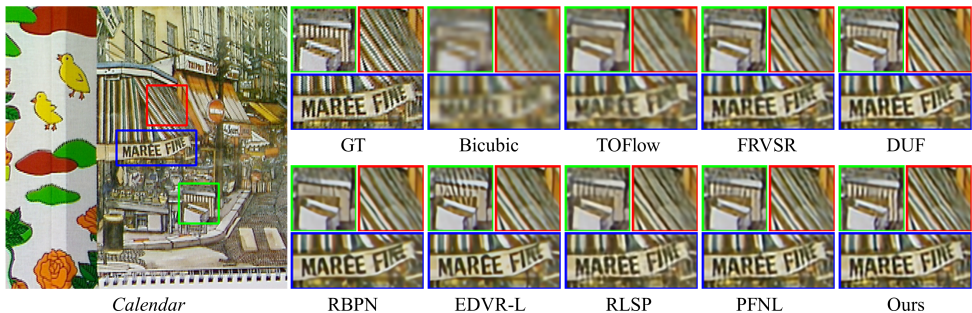


Figure 1: $\times 4$ VSR results for the scene *Calendar* in Vid4 [19] dataset. Our method produces sharper edges and more detailed textures than other state-of-the-art methods.

2 Related work

Single image super-resolution. With the development of deep learning, the convolutional neural network method has achieved dramatic advantages against conventional methods in single image super-resolution (SISR). In [8], Deng *et al.* first proposed to use a 3-layer end-to-end convolutional neural network to fill the missing details of the interpolated low-resolution images and showed promising results. Since then, there have been numerous learning-based SISR methods [7, 14, 15, 22, 29, 30] constantly emerging. VDSR [14] further improved CNN depth by stacking more convolutional layers with global residual learning. DRCN [15] first proposed to reduce model parameters with recursive learning in deep CNN. However, DRCN also suffers from performance degradation problems when increasing more convolutional layers (up to 16 convolutional recursions). To further increase CNN depth, DRRN [22] was proposed with local residual learning and global residual learning strategy. Much deeper CNN, including RDN [30], DBPN [7], RCAN [29] were then introduced, which outperformed previous works by a large margin. In this paper, we also enjoy the merits of residual learning and incorporate residual connection in the Recurrent neural network (RNN). The proposed RRN not only carries rich details from the previous layers to later layers in the hidden state, where information can be stably propagated even through a large number of convolutional layers but also carries on historical information through a long range of time steps as the additional complementary information for the later time step.

Video super-resolution. Temporal modeling plays a key role in VSR. Previous works performing temporal aggregation fall into three branches: 1) 2D CNN with early fusion [8, 24, 25, 27] 2) 3D CNN with slow fusion [12, 16] and 3) RNN based [9, 20] methods. TDAN [24] and EDVR [25] aggregated multi-frames features with several 2D convolutional layers on the top of the feature-wise alignment. PFNL [27] captured long-range dependencies through a kind of non-local operation, and then aggregated the correlations maps with several 2D convolutional layers. Kim *et al.* used several stacked 3D convolutional layers to extract both spatial and temporal information within a temporal sliding window in a slow fusion manner and implemented this fashion over the entire video sequence. DUF [12] estimated dynamic filters with stacked 3D convolutional layers for implicit motion compensation and upsampling. With the advanced temporal modeling strategy, CNN based methods show superior performance on several benchmarks. However, the overlap of sliding windows leads to redundant computation, which limits the VSR efficiency. As for recurrent based methods, both historical information across time step and current information between consecutive frames

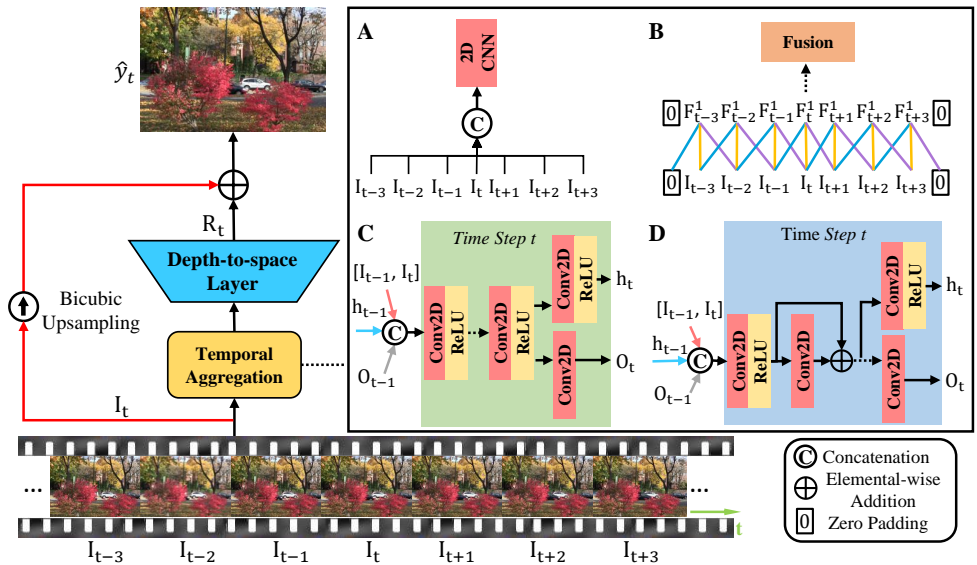


Figure 2: Schematic illustration of three commonly used temporal modeling frameworks (A: 2D CNN with early fusion, B: 3D CNN with slow fusion, C: RNN). D is the proposed RRN.

can be used to enhance details for an LR frame. In [20], Sajjadi *et al.* proposed to conduct motion estimation and warp operation between the previous frame and current frame, and then super-resolve the aligned frame in a recurrent manner. However, inaccurate motion estimation would cause severe artifacts and increase the risk of error accumulation. Recently, Fouli *et al.* proposed RLSP [9], which propagated historical information in feature space and without explicit motion estimation. Related to [9], our method also propagates historical information in feature space. However, in [9], they adopt seven simply connected convolutional layers as the hidden state, which is difficult to preserve texture details when propagate so many layers in the hidden state. In addition, RLSP fed three consecutive frames into each hidden state. With more input frames, the hidden state would easily suffers from error accumulation, especially when there is large motion between consecutive frames. In this work, we exploit two frames (previous and current) as hidden state input, and incorporate identity mapping in hidden state to preserve the texture details through so many layers.

3 Methodology

3.1 Overview

In this section, we introduce the overall system pipeline and detailed configurations of the temporal modeling methods. The whole system consists of two parts: a temporal modeling network which takes consecutive frames as input and integrates them with the reference frame, and a loss function to optimize the network utilizing motion information in an implicit manner. We comprehensively study and compare three temporal modeling methods, including 2D CNN with early fusion, 3D CNN with slow fusion and RNN. Schematic illustration of these networks is shown in Fig. 2 (a), (b) and (c), respectively. The detailed architecture about the proposed hidden state is shown in Fig. 2 (d).

3.2 Network Design

We consider three types of deep neural networks: (1) 2D CNN (2) 3D CNN and (3) RNN. For 2D CNN, the input frames are first concatenated along the channel axis, and then aggregated with a stack of 2D convolutional layer. 3D CNN takes a video sequence as input and then exploits a stack of 3D convolutional layer to extract the spatial-temporal information from the video sequence. Comparing to the CNN methods, RNN takes fewer frame as the hidden state input and handles a long video sequence with a recurrent manner.

2D CNN with early fusion.

Inspired by [18], we design the 2D CNN with several modified 2D residual blocks, where each block consists of a 3×3 convolutional layer followed by ReLU [5]. Such model takes $2T + 1$ consecutive frames as input. The aggregation process can be formulated as:

$$R_t = W_{net2D}\{W_{fusion2D}[I_{t-T}, \dots, I_{t+T}]\} \quad (1)$$

Where $[\cdot, \cdot, \cdot]$ denotes the concatenation operation. The input tensor shape of $W_{fusion2D}$ is $NC \times H \times W$, where $N = 2T + 1$, C is the number of color channels, and H, W are the height and weight of the input LR frames, respectively. $W_{fusion2D}$ and W_{net2D} represent a set of weights (the biases are omitted to simplify notations) of the early fusion layer and 2D CNN, respectively. The shape of the produced residual map is R_t is $H \times W \times Cr^2$, where r is the upscale factor. The high-resolution residual maps R_t^\uparrow is obtained by adopting depth-to-space operation [20]. Finally, the high-resolution image \hat{y}_t is obtained by adding the predicted high-resolution residual map R_t^\uparrow to a bicubic up-sampled high-resolution reference image I_t^\uparrow at the end of the network.

3D CNN with slow fusion. In 3D CNN, we modify the 2D convolutional layers in the 2D residual blocks to $3 \times 3 \times 3$ convolutional layers for extracting spatial-temporal information. We use the same network depth for both 2D and 3D CNN for a fair comparison. In contrast with 2D CNN, 3D CNN takes a video sequence as input and extracts the spatial-temporal information in a slow fusion manner. Specifically, a 3-dimensional filter moves both in temporal and spatial axis directions to extract both spatial and temporal information. Typically, the temporal dimension depth of 3D filter is much smaller than the length of the input sequence. Such slow fusion process can be described as:

$$R_t = W_{fusion3D}\{W_{net3D}\{I_{t-T:t+T}\}\} \quad (2)$$

Where W_{net3D} and $W_{fusion3D}$ represent a set of weights (the biases are omitted to simplify notations) of 3D CNN and the later fusion layer, respectively. The input tensor shape of W_{net3D} is $C \times N \times H \times W$, where C is the number of color channels, $N = 2T + 1$, and H, W are the height and weight of the input LR frames, respectively. To prevent the number of frames from decreasing, we add two frames with pixel value of zero in the temporal axis.

RNN. Typically, a hidden state at time step t takes three parts as input: (1) the previous output o_{t-1} , (2) the previous hidden state features h_{t-1} and (3) two adjacent frames $I_{\{t-1, t\}}$. Intuitively, in an video sequence, pixels within successive frames usually bear a strong similarity. The high-frequency texture details in t -th time step should be further refined by borrowing the complementary information from the previous layer. However, RNN in VSR [4] also suffers gradient vanishing issue as many other video processing tasks [2, 6, 23]. To address this issue, we propose a novel recurrent network, termed as Residual Recurrent Network (RRN), which adopts residual mapping between layers with identity skip connections. Such design ensures a fluent information flow and has the ability to preserve the texture information over long periods making RNN easier to process a longer sequences, and meanwhile

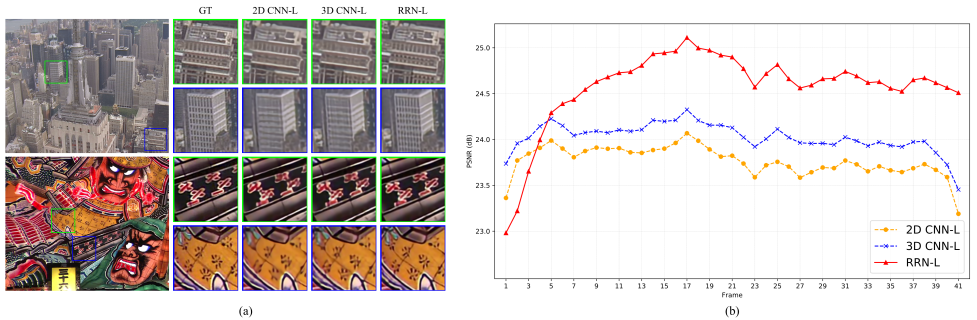


Figure 3: (a): Qualitative results for different temporal modeling methods on **Vid4** [19] and **SPMCS** [23] dataset for $4\times$ VSR. (b): Information flow over time for 2D CNN, 3D CNN and RNN on the *Calendar* sequence.

reduce the risk of gradient vanishing in training. At time step t , the RRN uses following equations to generate output h_t and o_t for the next time step $t+1$:

$$\begin{aligned} \hat{x}_0 &= \sigma(W_{conv2D}\{[I_{t-1}, I_t, o_{t-1}, h_{t-1}]\}) & \hat{x}_k &= g(\hat{x}_{k-1}) + \mathcal{F}(\hat{x}_{k-1}), k \in [1, K] \\ h_t &= \sigma(W_{conv2D}\{\hat{x}_K\}) & o_t &= W_{conv2D}\{\hat{x}_K\} \end{aligned} \quad (3)$$

Where $\sigma(\cdot)$ represents the ReLU function. $g(\hat{x}_{k-1})$ denotes an identity mapping in k -th residual block: $g(\hat{x}_{k-1}) = \hat{x}_{k-1}$, and $\mathcal{F}(\hat{x}_{k-1})$ denotes the residual mapping to be learned.

4 Experiment

4.1 Dataset

Previous works use different training sets and different down-sampling kernels, which restricts fair comparisons. In this work, we adopt Vimeo-90k [26] as the training set. Vimeo-90k is a public dataset for video restoration tasks, including video denoising, deblurring as well as super-resolution. Vimeo-90k contains around 90k 7-frame video clips with various motions and diverse scenes. To develop our model, the low-resolution patches in the size of 64×64 are obtained by applying Gaussian blur with $\sigma = 1.6$ to a high-resolution frame and further downsampling by $4\times$ scale factor. We evaluate the developed models on Vid4 [19], SPMCS [23] and UDM10 [27] datasets. Vid4 consists of four scenes with various motion and occlusion. SPMCS and UDM10 are the recently proposed validation sets, which contain diverse senses with considerable high-resolution frames than Vid4.

4.2 Implementation Details

We consider two models which have different network depth for all temporal modeling method.

As for 2D CNN, 2D CNN-S, 2D CNN-L adopt five and ten 2D residual blocks, respectively. As for 3D CNN, 3D CNN-S and 3D CNN-L adopt five and ten 3D residual blocks, respectively.

Method	2D CNN S	3D CNN S	RRN S	2D CNN L	3D CNN L	RRN L
Blocks	5	5	5	10	10	10
Input Frames	7	7	recurrent	7	7	recurrent
# Param. [M]	2.8	5.5	1.9	4.3	9.9	3.4
FLOPs [GMAC]	395	1852	108	480	3640	193
Vid4 (Y)	26.72	27.08	27.38	26.96	27.25	27.69
SPMCS (Y)	29.05	29.42	29.48	29.51	29.64	29.84
UDM10 (Y)	37.67	38.12	38.33	38.15	38.43	38.97
Runtime [ms]	97	558	30	116	1045	45

Table 1: Comparison of PSNR values on Vid4 [19], SPMCS [23] and UDM10 [27] and runtime between different temporal modeling methods for $\times 4$ VSR. Y denotes the evaluation on luminance channel. Runtime is calculated on an LR image of size 320×180 . Red text indicates the best and blue text indicates the second best performance. Best view in color.

The channel size for 2D CNN and 3D CNN is set to 128. For a fair comparison with the CNN based methods, we also adopt five and ten residual blocks as the hidden state for RRN-S and RRN-L, respectively. Each block consists of a convolutional layer, a ReLU layer and following another convolutional layer. The channel size of convolutional layer is set to 128. At the time step t_0 , the previous estimation is initialized with zero. To train the CNN based models, the learning rate is initially set to 1×10^{-4} and 1×10^{-3} for 2D CNN and 3D CNN, respectively, and multiplied by 0.1 after 10 epochs. The training step completes after 30 epochs. To train the RNN based model, the learning rate is initially set to 1×10^{-4} and later down-scaled by a factor of 0.1 every 60 epoch till 70 epochs. All models are supervised by pixel-wise \mathcal{L}_1 loss function with Adam [17] optimizer by setting $\beta_1 = 0.9$, $\beta_2 = 0.999$ and weight decay of 5×10^{-4} . We set the size of mini-batch as 64 and 4 for CNN based and RNN based methods, respectively. The \mathcal{L}_1 loss is applied on all pixels between the ground truth frames y_t^* and the network’s output \hat{y}_t , defined by $\mathcal{L} = \|y_t^* - \hat{y}_t\|$. All experiments are conducted using Python 3.6.4 and Pytorch 1.1.

4.3 Comparison with different temporal modeling methods

In this part, we compare three temporal modeling approaches, including 2D CNN, 3D CNN and RNN on Vid4 [19], SPMCS [23] and UDM10 [27] datasets. The quantitative and qualitative results are shown in Tab. 1 and Fig. 3, respectively. We also present the trade-off between runtime and accuracy in Tab. 1.

In CNN-based methods, 3D CNN-S and 3D CNN-L outperform 2D CNN-S and 2D CNN-L by a large margin. However, VSR with 3D CNN is very time-consuming as shown in Tab. 1, where 3D CNN-L is almost ten times slower than 2D CNN-L on processing an LR frame of size 320×180 . Comparing with CNN based methods, RNN is highly computational efficiency and achieves excellent results with fewer parameters. RRN-L is 0.44, 0.20 and 0.54 dB higher than 3D CNN-L on Vid4, SPMCS and UDM10, respectively, and meanwhile being more than $23 \times$ faster. Moreover, RNN-S and RNN-L can produce a 720p video sequences in 33fps and 22fps, respectively. The qualitative results also show that RRN-L can produce finer details and fewer artifacts than 2D CNN-L and 3D CNN-L. In addition, we visualize the temporal profiles in Fig. 5. RRN-L produces temporal consistent frames and suffers less flickering artifacts than other temporal modeling methods.

To investigate the information flow of different temporal modeling methods for handling a

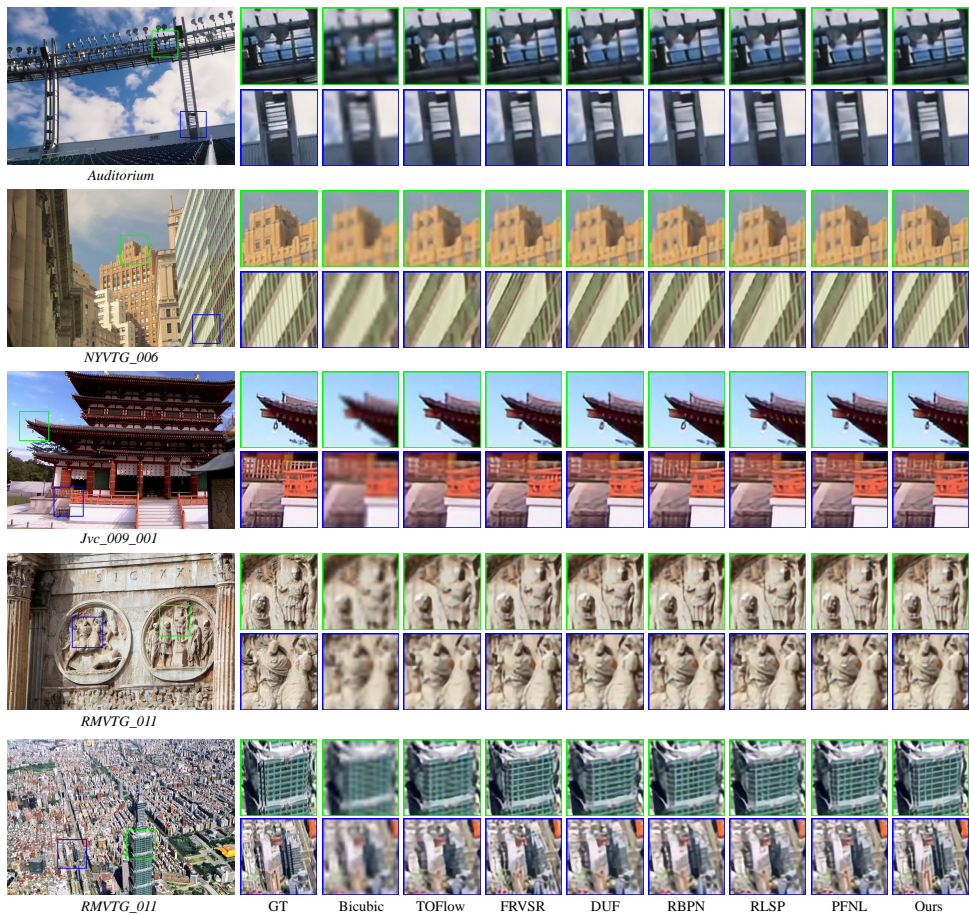


Figure 4: Qualitative comparison on the UDM10 [27] and SPMCS [23] datasets for $4\times$ VSR. Zoom in for better visualization.

long video sequence, we plot the PSNR over time for *Calendar* sequence in Vid4. As shown in Fig. 3 (b), the RNN-based method falls behind the CNN-based methods at the first five frames. By accumulating information over time, the RNN-based method outperforms CNN-based methods from the fifth frame. More interestingly, the CNN-based methods suffer from performance degradation at the fifth frames, but the RNN-based method keeps improving, which demonstrates that the information accumulation in the previous hidden state provides a complementary information for recovering missing details.

Necessity of residual connection in the hidden state of RNN. To investigate the necessity of residual learning in the hidden state, we create a simple baseline by removing by simply stacking the convolutional layer in a hidden state. The advanced model is obtained by incorporating the identity mapping in a hidden state. The PSNR (dB) and SSIM results on Vid4 are shown in Tab. 2. The quantitative results are measured on the luminance (Y) channel. As shown in Tab. 2, the best performance of the baseline model is 27.09 dB in PSNR, which uses three blocks as the hidden state. However, it suffers from gradient vanishing when increasing the number of blocks to the number of four. With the help of a residual connection in the hidden state, stable improvement is achieved when increasing the number

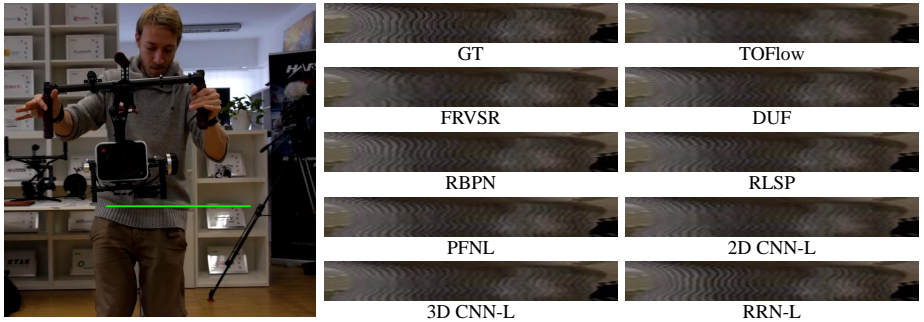


Figure 5: Visualization of temporal consistency for the *Photography* sequence in UDM10 [27]. The temporal profile is produced by recording a single-pixel line (green line) spanning time and stacked vertically.

of blocks. These results illustrate that identity mapping can not only stabilize training but also boost the VSR performance. Note that the performance of RRN can be further improved by adopting more blocks.

Blocks	2	3	4	5	6	7	8	9	10
RRN w/o residual	26.70/0.8050	26.75/0.8108	*	*	*	*	*	*	*
RRN w/ residual	26.97/0.8119	27.09/0.8286	27.20/0.8334	27.38/0.8385	27.42/0.8434	27.53/0.8433	27.65/0.8468	27.67/0.8476	27.69/0.8488

Table 2: Ablation on the residual learning in the hidden state of RRN. “*” represents that the model in training suffers from gradient vanishing.

4.4 Comparison with state-of-the-art methods

We compare our best model (RRN-L) with eight state-of-the-art VSR approaches: SPMC [23], TOFlow [26], FRVSR [20], DUF [12], RBPN [8], EDVR [25], RLSP [9] and PFNL [27]. SPMC, TOFlow and FRVSR apply for explicit motion estimation and compensation. EDVR conducts motion alignment in feature level. RBPN also computes optical flow but uses it as additional input instead of explicit motion compensation. DUF and PFNL use an advanced temporal integration network to utilize motion information in an implicit way. RLSP is the most related work, which also propagates historical information in feature space. However, the design of the hidden state of RLSP is simple, which easily causes gradient vanishing problem (see Tab 2). Most of the previous methods use different training sets and different down-sampling operations. For fair comparison, we fix the down-sampling filters, *i.e.* $\sigma = 1.6$, and carefully re-implement these methods on the public Vimeo-90k dataset. The quantitative results on Vid4, SPMCS and UDM10 are shown in Tab. 3. We can see that methods with explicit motion compensation do not perform very well. By carefully analyzing, the occlusion or complex motion easily influences the per-pixel motion estimation, such as optical flow. Inaccurate motion estimation would introduce artifacts which deteriorate super-resolution performance. As shown in Tab. 3, our method outperforms the CNN-based methods [8, 12, 23, 25, 26, 27] by a large margin, and meanwhile runs been $70\times$ and $6\times$ faster than the recent proposed RBPN and PFNL, respectively. Comparing with other RNN-based methods [9, 20], our method outperforms FRVSR by a large margin even with fewer parameters and $2\times$ faster. Our method achieves comparable runtimes with RLSP, but it outperforms RLSP by 0.21, 0.25 and 0.48 dB in PSNR on Vid4, SPMCS and UDM10, respectively. Qualitative comparisons are presented in Fig. 4. The proposed method produces

Method	Bicubic	SPMC [†] [1]	TOFLOW [2]	FRVSR [3]	DUF [4]	RBPN [5]	EDVR [6]	RLSP [7]	PFNL [8]	RRN-L (Ours)
# Param. [M]	N/A	-	1.4	5.1	5.8	12.8	20.1	4.3	3.0	3.4
Runtime [ms]	N/A	-	1658	129	1393	3482	621	50	295	45
Vid4 (Y)	21.80/0.5426	25.52/0.76	25.85/0.7659	26.48/0.8104	27.38/0.8329	27.17/0.8205	27.35/0.8264	27.48/0.8388	27.16/0.8365	27.69/0.8488
Vid4 (RGB)	20.37/0.5106	-/-	24.39/0.7438	25.01/0.7917	25.91/0.8166	25.65/0.7997	25.83/0.8077	25.69/0.8153	25.67/0.8189	26.16/0.8209
SPMCS (Y)	23.29/0.6385	-/-	27.86/0.8237	28.16/0.8421	29.63/0.8719	29.73/0.8663	-/-	29.59/0.8762	29.74/0.8792	29.84/0.8827
SPMCS (RGB)	21.83/0.6133	-/-	26.38/0.8072	26.68/0.8271	28.10/0.8582	28.23/0.8561	-/-	27.25/0.8495	27.24/0.8495	28.28/0.8690
UDM10 (Y)	28.47/0.8523	-/-	36.26/0.9438	37.09/0.9522	38.48/0.9605	38.66/0.9596	-/-	38.48/0.9606	38.74/0.9627	38.96/0.9644
UDM10 (RGB)	27.05/0.8267	-/-	34.46/0.9298	35.39/0.9403	36.78/0.9514	36.53/0.9462	-/-	36.39/0.9465	36.91/0.9526	37.03/0.9534

Table 3: Quantitative comparison (PSNR(dB) and SSIM) on Vid4 [19], SPMCS [23] and UDM10 [24] for 4×VSR, respectively. ‘†’ means the values are taken from original publications or calculated by provided models. Y and RGB indicate the evaluation on luminance channel or RGB channels, respectively. Runtime is calculated on an LR image of size 320×180. Red text indicates the best and blue text indicates the second best performance. Best view in color.

sharper edges and finer details than other VSR methods. In addition, our method produces temporal-consistent results than the previous methods, as shown in Fig. 5

5 Conclusion

Video super-resolution is an important task, which has drawn much attention in both research and industrial communities. We comprehensively investigate and compare three commonly used temporal modeling methods for video super-resolution, including 2D CNN with early fusion, 3D CNN with slow fusion and RNN. For a fair comparison, all models are developed on the public Vimeo-90k dataset with the fixed down-sampling filters and loss function. Extensive experiments on Vid4, SPMCS and UDM10 benchmarks, demonstrate RNN is highly efficient and benefit in dealing with the VSR problem. In addition, we also propose a novel hidden state structure for recurrent network, termed as RRN. The proposed method achieves state-of-the-art performance on three benchmarks.

Acknowledgement

This work was supported in part by the National Natural Science Foundation of China under Grant 61701277 and Grant 61771288 and in part by the State Key Development Program in 13th Five-Year under Grant 2017YFC0821601.

References

- [1] Jose Caballero, Christian Ledig, Andrew Aitken, Alejandro Acosta, Johannes Totz, Zehan Wang, and Wenzhe Shi. Real-time video super-resolution with spatio-temporal networks and motion compensation. In *CVPR*, 2017.
- [2] Jingwen Chen, Yingwei Pan, Yehao Li, Ting Yao, Hongyang Chao, and Tao Mei. Temporal deformable convolutional encoder-decoder networks for video captioning. In *Proceedings of the AAAI Conference on Artificial Intelligence*, 2019.
- [3] Chao Dong, Chen Change Loy, Kaiming He, and Xiaoou Tang. Learning a deep convolutional network for image super-resolution. In *ECCV*, 2014.
- [4] Dario Fuoli, Shuhang Gu, and Radu Timofte. Efficient video super-resolution through recurrent latent space propagation. *CoRR*, abs/1909.08080, 2019.

-
- [5] Xavier Glorot, Antoine Bordes, and Yoshua Bengio. Deep sparse rectifier neural networks. In *AISTATS*, 2011.
- [6] Daniel Gordon, Ali Farhadi, and Dieter Fox. Re3: Re al-time recurrent regression networks for visual tracking of generic objects. *IEEE Robotics and Automation Letters*, 3(2):788–795, 2018.
- [7] Muhammad Haris, Gregory Shakhnarovich, and Norimichi Ukita. Deep back-projection networks for super-resolution. In *CVPR*, 2018.
- [8] Muhammad Haris, Gregory Shakhnarovich, and Norimichi Ukita. Recurrent back-projection network for video super-resolution. In *CVPR*, 2019.
- [9] Yan Huang, Wei Wang, and Liang Wang. Bidirectional recurrent convolutional networks for multi-frame super-resolution. In *NeurIPS*, 2015.
- [10] Takashi Isobe, Xu Jia, Shuhang Gu, Songjiang Li, Shengjin Wang, and Qi Tian. Video super-resolution with recurrent structure-detail network. 2020.
- [11] Takashi Isobe, Songjiang Li, Xu Jia, Shanxin Yuan, Gregory Slabaugh, Chunjing Xu, Ya-Li Li, Shengjin Wang, and Qi Tian. Video super-resolution with temporal group attention. In *CVPR*, 2020.
- [12] Younghyun Jo, Seoung Wug Oh, Jaeyeon Kang, and Seon Joo Kim. Deep video super-resolution network using dynamic upsampling filters without explicit motion compensation. In *CVPR*, 2018.
- [13] Armin Kappeler, Seunghwan Yoo, Qiqin Dai, and Aggelos K Katsaggelos. Video super-resolution with convolutional neural networks. *IEEE Transactions on Computational Imaging*, 2(2):109–122, 2016.
- [14] Jiwon Kim, Jung Kwon Lee, and Kyoung Mu Lee. Accurate image super-resolution using very deep convolutional networks. In *CVPR*, 2016.
- [15] Jiwon Kim, Jung Kwon Lee, and Kyoung Mu Lee. Deeply-recursive convolutional network for image super-resolution. In *CVPR*, 2016.
- [16] Soo Ye Kim, Jeongyeon Lim, Taeyoung Na, and Munchurl Kim. 3dsrnet: Video super-resolution using 3d convolutional neural networks. *CoRR*, abs/1812.09079, 2018.
- [17] Diederik P. Kingma and Jimmy Ba. Adam: A method for stochastic optimization. In *ICLR*, 2015.
- [18] Bee Lim, Sanghyun Son, Heewon Kim, Seungjun Nah, and Kyoung Mu Lee. Enhanced deep residual networks for single image super-resolution. In *CVPR Workshops*, 2017.
- [19] Ce Liu and Deqing Sun. On bayesian adaptive video super resolution. *IEEE transactions on pattern analysis and machine intelligence*, 36(2):346–360, 2013.
- [20] Mehdi SM Sajjadi, Raviteja Vemulapalli, and Matthew Brown. Frame-recurrent video super-resolution. In *CVPR*, 2018.

- [21] Wenzhe Shi, Jose Caballero, Ferenc Huszár, Johannes Totz, Andrew P Aitken, Rob Bishop, Daniel Rueckert, and Zehan Wang. Real-time single image and video super-resolution using an efficient sub-pixel convolutional neural network. In *CVPR*, 2016.
- [22] Ying Tai, Jian Yang, and Xiaoming Liu. Image super-resolution via deep recursive residual network. In *CVPR*, 2017.
- [23] Xin Tao, Hongyun Gao, Renjie Liao, Jue Wang, and Jiaya Jia. Detail-revealing deep video super-resolution. In *ICCV*, 2017.
- [24] Yapeng Tian, Yulun Zhang, Yun Fu, and Chenliang Xu. Tdan: Temporally deformable alignment network for video super-resolution. *CoRR*, abs/1812.02898, 2018.
- [25] Xintao Wang, Kelvin CK Chan, Ke Yu, Chao Dong, and Chen Change Loy. Edvr: Video restoration with enhanced deformable convolutional networks. In *CVPR Workshops*, 2019.
- [26] Tianfan Xue, Baian Chen, Jiajun Wu, Donglai Wei, and William T Freeman. Video enhancement with task-oriented flow. *International Journal of Computer Vision*, 127(8):1106–1125, 2019.
- [27] Peng Yi, Zhongyuan Wang, Kui Jiang, Junjun Jiang, and Jiayi Ma. Progressive fusion video super-resolution network via exploiting non-local spatio-temporal correlations. In *ICCV*, 2019.
- [28] Pengfei Zhang, Jianru Xue, Cuiling Lan, Wenjun Zeng, Zhanning Gao, and Nanning Zheng. Eleatt-rnn: Adding attentiveness to neurons in recurrent neural networks. *IEEE Transactions on Image Processing*, 2019.
- [29] Yulun Zhang, Kunpeng Li, Kai Li, Lichen Wang, Bineng Zhong, and Yun Fu. Image super-resolution using very deep residual channel attention networks. In *ECCV*, 2018.
- [30] Yulun Zhang, Yapeng Tian, Yu Kong, Bineng Zhong, and Yun Fu. Residual dense network for image super-resolution. In *CVPR*, 2018.